

## Journal: NETWORK NEUROSCIENCE

### 1 RESEARCH

## 2 Similarity in evoked responses does not imply similarity in macroscopic 3 network states

4 **Javier Rasero<sup>1,2,3</sup>, Richard Betzel<sup>4</sup>, Amy Isabella Sentis<sup>2,5</sup>, Thomas E. Kraynak<sup>5,6</sup>, Peter J. Gianaros<sup>5,6</sup>  
5 and Timothy Verstynen<sup>1,2,5,7</sup>**

6 <sup>1</sup>Department of Psychology, Carnegie Mellon University, Pittsburgh, PA 15213, USA

7 <sup>2</sup>Neuroscience Institute, Carnegie Mellon University, Pittsburgh, PA 15213, USA

8 <sup>3</sup>School of Data Science, University of Virginia, Charlottesville, VA 22902, USA

9 <sup>4</sup>Department of Psychological and Brain Sciences, Indiana University, Bloomington, IN 47405, USA

10 <sup>5</sup>Center for the Neural Basis of Cognition, University of Pittsburgh and Carnegie Mellon University, Pittsburgh, PA 15213, USA

11 <sup>6</sup>Department of Psychology, University of Pittsburgh, Pittsburgh, PA 15260, USA

12 <sup>7</sup>Biomedical Engineering, Carnegie Mellon University, Pittsburgh, PA 15213, USA

13 **Keywords:** Modular Brain, Dynamical Systems, fMRI, Instantaneous Connectivity, Brain Activation

### ABSTRACT

14 It is commonplace in neuroscience to assume that if two tasks activate the same brain areas in the same  
15 way, then they are recruiting the same underlying networks. Yet computational theory has shown that the  
16 same pattern of activity can emerge from many different underlying network representations. Here we  
17 evaluated whether similarity in activation necessarily implies similarity in network architecture by  
18 comparing region-wise activation patterns and functional correlation profiles from a large sample of  
19 healthy subjects (N=242) that performed two executive control tasks known to recruit nearly identical  
20 brain areas, the color-word Stroop task and the Multi-Source Interference Task (MSIT). Using a measure  
21 of instantaneous functional correlations, based on edge time series, we estimated the task-related

22 networks that differed between incongruent and congruent conditions. We found that the two tasks were  
 23 much more different in their network profiles than in their evoked activity patterns at different analytical  
 24 levels, as well as for a wide range of methodological pipelines. Our results reject the notion that having  
 25 the same activation patterns means two tasks engage the same underlying representations, suggesting that  
 26 task representations should be independently evaluated at both node and edge (connectivity) levels.

## AUTHOR SUMMARY

27 As a dynamical system, the brain can encode information at the module (e.g., brain regions) or the  
 28 network level (e.g., connections between brain regions). This means that two tasks can produce the same  
 29 pattern of activation, but differ in their network profile. Here we tested this using two tasks with largely  
 30 similar cognitive requirements. Despite producing nearly identical macroscopic activation patterns, the  
 31 two tasks produced more different functional network profiles. These findings confirm prior  
 32 theoretical work that similarity in task activation does not imply the same similarity in underlying  
 33 network states.

## INTRODUCTION

34 The idea of a modular mind (Fodor, 1983), where cognition arises from the interplay between  
 35 specialized, domain-specific units that represent fundamental cognitive processes, has dominated the  
 36 cognitive neuroscientific view of the brain since its inception (e.g., Posner, Petersen, Fox, and Raichle  
 37 (1988)). Here the cognitive "modules" are mapped to unique brain areas that execute specific processes  
 38 (e.g., detecting specific sound frequencies, estimating value, contracting specific muscle groups)  
 39 (Feinberg & Farah, 2006). Over the last four decades, this modular view of the brain has largely been  
 40 justified by empirical observations using non-invasive brain imaging methods, like positron emission  
 41 tomography and functional MRI (fMRI), where experiments and analytical methods were explicitly  
 42 designed to isolate clusters of regions aligned to certain functional domains, such as vision (e.g., Bihani et  
 43 al. (1993)), control (e.g., Porro et al. (1996)), language (e.g., Binder et al. (1997)), or affect (e.g., Anders,  
 44 Lotze, Erb, Grodd, and Birbaumer (2004)).

45 As a consequence of this early modularist perspective, as well as limitations of early brain imaging  
46 technology, a large part of early cognitive neuroscience focused on what was happening at these modules  
47 themselves. Many inferences focused on which regions were activated (or deactivated) by specific task  
48 conditions. This often led to the implicit assumption that if the same brain regions were activated by two  
49 different tasks, then the tasks relied on the same brain networks and, thus, the same underlying cognitive  
50 processes. Yet, with the rise of the dynamical systems perspective of the brain (Gelder, 1995; Kelso,  
51 1995), it became increasingly clear that understanding the modules is not enough. In order to understand  
52 how tasks are internally represented one must understand the interactions between modules as well. This  
53 dynamical systems perspective has gained ground over the past decade in systems neuroscience, where  
54 multi-unit recording studies have shown that task representations emerge as a low-dimensional manifold  
55 of population activity, both within and between brain areas (Churchland et al., 2012; Oby et al., 2019;  
56 Russo et al., 2020; Sadtler et al., 2014). This observation at the microscale level extends to observations  
57 of macroscopic brain dynamics as well (e.g., Ejaz, Hamada, and Diedrichsen (2015); Kriegeskorte et al.  
58 (2008)). With the rise of connectomics Behrens and Sporns (2012), the idea of the brain as a dynamical  
59 network Sporns (2013), where information is also encoded *between* units (Bertolero, Yeo, & D'Esposito,  
60 2015; Crossley et al., 2013; Yeo et al., 2014), has proven to be incredibly useful at explaining both  
61 underlying representations and brain-behavior relationships.

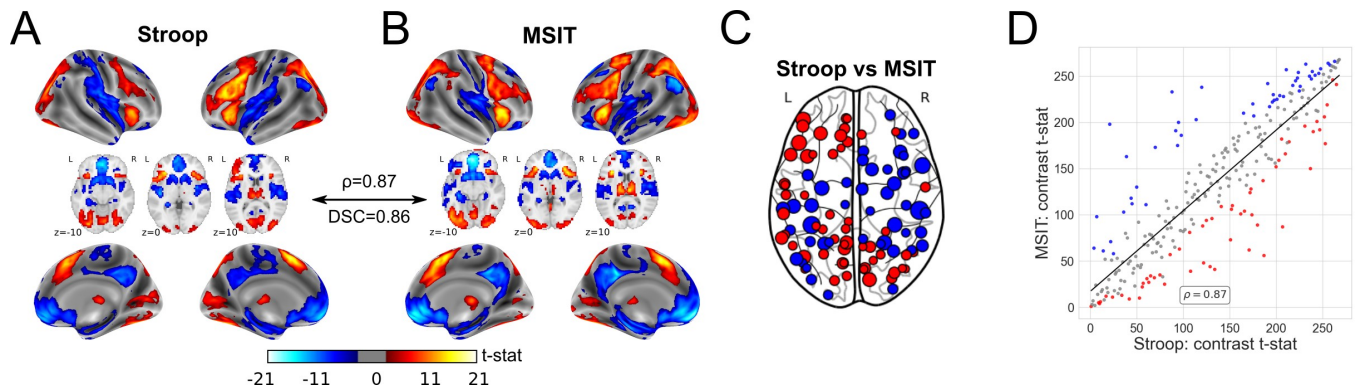
62 One interesting consequence of this network-level perspective is the decoupling of activation patterns  
63 from underlying network states: two tasks can produce the same patterns of activity in the same brain  
64 regions, but have fundamentally different underlying network profiles. Indeed, Prinz and colleagues  
65 (2004) illustrated this using a simple three unit computational model of stomatogastric ganglia in lobsters  
66 (Prinz, Bucher, & Marder, 2004). Simply by varying the relative connection weights between the three  
67 units, the authors showed how multiple underlying network states can be realized as identical patterns of  
68 activity at the units themselves. Here we test the predictions of Prinz and colleagues (2004), at the  
69 macroscopic level, by measuring blood oxygen level-dependent (BOLD) dynamics elicited during two  
70 response conflict tasks, the color-word Stroop task (Stroop, 1935) and the Multi-Source Interference Task  
71 (MSIT) (Bush & Shin, 2006). This develops on previous work exploring the relationship between task  
72 activation and functional correlations (Alnæs et al., 2015; Chan, Alhazmi, Park, Savalia, & Wig, 2017;  
73 Gratton, Laumann, Gordon, Adeyemo, & Petersen, 2016; Krienen, Yeo, & Buckner, 2014; Newton,

<sup>74</sup> Morgan, Rogers, & Gore, 2010; Spadone et al., 2015), but concentrating on these two tasks because they  
<sup>75</sup> share common computational demands and have overlapping topologies of evoked responses (Sheu,  
<sup>76</sup> Jennings, & Gianaros, 2012). In a sample of neurologically healthy adults (N=242), we first computed  
<sup>77</sup> instantaneous functional correlation graphs, using a novel approach that temporally unwraps Pearson  
<sup>78</sup> correlations to generate time series along edges, representing the inter-node BOLD signal co-fluctuations  
<sup>79</sup> (Zamani Esfahlani et al., 2020). Then, by means of a general linear model (GLM), we assessed the  
<sup>80</sup> task-based contributions to the edge time series, quantifying the amount of out-of-sample variability that  
<sup>81</sup> they contained. We then compared the degree of between-task similarity at the regional activation and  
<sup>82</sup> connectomic levels.

## RESULTS

### <sup>83</sup> *Group-level activation patterns*

<sup>84</sup> We begin by replicating an exhaustively reported effect (see Sheu et al. (2012) and references in), namely  
<sup>85</sup> that the Stroop task and MSIT, both effortful cognitive control tasks, have largely overlapping spatial  
<sup>86</sup> patterns of evoked activity across the brain, particularly the neocortex (see contrasts maps in Fig. 1A and  
<sup>87</sup> B). Here such similarity was quantified by a Spearman's correlation coefficient,  $\rho$ , between  
<sup>88</sup> un-thresholded incongruent-vs-congruent t-stat maps calculated at the region-level (voxel-wise  
<sup>89</sup> estimations with the same region-size spatial smoothing yielded similar values), and a Dice similarity  
<sup>90</sup> coefficient (DSC), from binarizing these maps as to whether their t-stats rejected or not the null  
<sup>91</sup> hypothesis at  $\alpha = 0.05$  after family-wise (Holm–Bonferroni) error correction. For our group-level  
<sup>92</sup> activation patterns, the former,  $\rho$ , was equal to 0.87, and the latter, DSC, was equal to 0.85. As shown in  
<sup>93</sup> Fig. 1A and B, increases in brain activity in incongruent trials, with respect to congruent trials, were  
<sup>94</sup> located in areas typically engaged during the processing of conflictual information and response  
<sup>95</sup> inhibition, such as the anterior cingulate cortex, anterior insula, parietal cortex, basal ganglia, thalamus,  
<sup>96</sup> and cerebellum. In contrast, de-activations took place in areas within the ventromedial prefrontal cortex,  
<sup>97</sup> perigenual anterior cingulate cortex, posterior cingulate cortex, and precuneus, which all comprise the  
<sup>98</sup> default-mode network. As a consequence, these results show that similar cognitive contexts evoke similar  
<sup>99</sup> patterns of activity across the brain. Nevertheless, both tasks also exhibited substantial differences in the  
<sup>100</sup> magnitude of their evoked responses, particularly in areas such as the dorsal and medial prefrontal cortex,

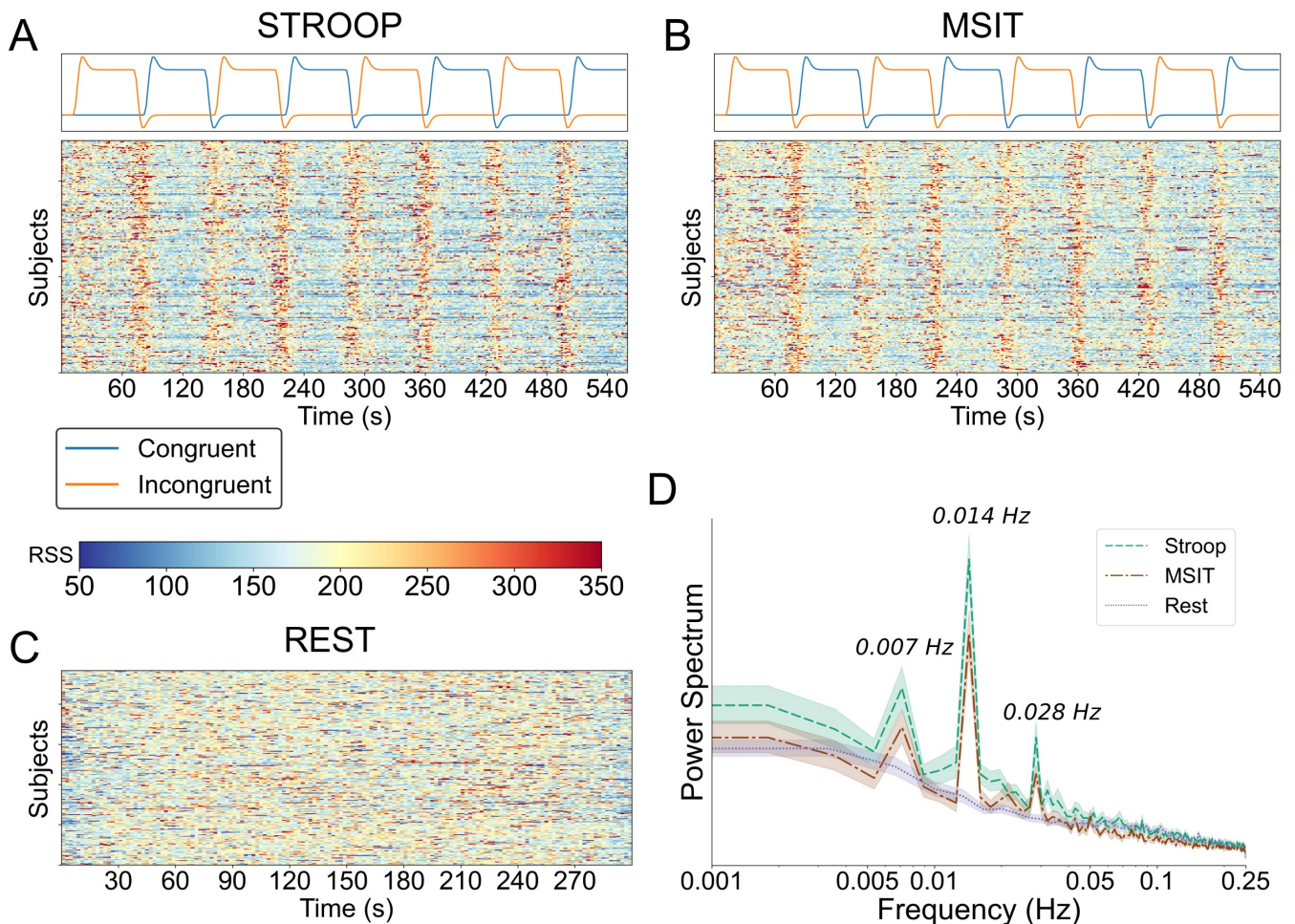


104 **Figure 1. Group-level activation maps.** For both Stroop task (A) and MSIT (B), the group-level incongruent-vs-congruent t-stat maps, at the voxel level  
 105 for aesthetic reasons. Thus, red colors display higher BOLD activity during incongruent trials compared to congruent trials, whereas blue colors represent the  
 106 other way around. C) Using a paired t-test at  $\alpha = 0.05$  (false-discovery rate corrected), between-task differences in activation patterns at the region level.  
 107 Red colors indicate greater incongruent-vs-congruent values in Stroop than MSIT, and blue colors the opposite. Bigger points correspond to bigger differences  
 108 between both tasks. D) The actual correlation comparing the group-level incongruent-vs-congruent t-stat maps of both tasks. Here, ranks are displayed instead  
 109 of the actual values, given that the similarity between spatial maps was measured by the Spearman's correlation. Red and blue colors correspond to the same  
 110 points displayed in (C), whereas gray-colored points represent those for which the evoked magnitude response did not significantly differ between the two  
 111 tasks.

101 post- and precentral gyrus, and the precuneus (see Fig. 1C). As expected, some of these regions were also  
 102 the most influential in the spatial correlation between the contrast maps of both tasks (those points further  
 103 away from the line in Fig. 1D).

### 112 *Exploration of co-fluctuating hemodynamics*

113 For illustrative purposes, we examined the task-related effects on the inter-region co-fluctuations by  
 114 computing the root sum of squares (RSS) across edges at each time frame. It is important to clarify that,  
 115 for this calculation, parcellated BOLD time series prior to edge time series formation included all task  
 116 events, in contrast to subsequent analyses. As shown in Fig. 2A and B, during both tasks moments of  
 117 high co-fluctuations tended to be synchronized across subjects, concentrated mostly around the rest  
 118 periods separating congruent and incongruent block conditions. In both the congruent and incongruent  
 119 blocks, there appeared to be a consistent reduction in global functional connectivity, with sporadic and



122 **Figure 2. Analysis of the root sum of squares time series.** For each subject, the root sum of squares of the edge time series that include the task effects for  
 123 Stroop task (A), MSIT (B) and resting-state acquisition (C). Their power spectrum (in arbitrary units) using a periodogram (D), averaged across subjects.

120 inconsistent periods of brief synchronous activity that qualitatively appear more frequent during  
 121 incongruent blocks.  
 124 In contrast to the task patterns, for the resting-state run, where no external stimulus was presented, we  
 125 did not see evidence of between-subject synchronization of high amplitude co-fluctuations (Fig. 2C).  
 126 Though the overall presence of these brief co-fluctuations appears to be qualitatively more frequent in the  
 127 resting-state run than during either of the two tasks. These results were further confirmed by inspecting

<sup>128</sup> the subject-averaged power spectrum of the RSS for the three tasks (Fig. 2D). For both Stroop and MSIT,  
<sup>129</sup> there was an overall increase in power at frequencies consistent with task onsets and offsets.

<sup>130</sup> ***Group-level functional correlations***

<sup>131</sup> We estimated task-related functional correlations using a GLM on the edge time series. Three coefficients  
<sup>132</sup> (i.e., intercept, congruent, and incongruent) for both Stroop task and MSIT were estimated for each edge,  
<sup>133</sup> while for resting state a single coefficient per edge was obtained (i.e., intercept only). The resulting  
<sup>134</sup> group-level network profiles are displayed in Fig. 3, where the t-stats for each of these coefficients were  
<sup>135</sup> converted to correlations using the transformation  $r^2 = \frac{t^2}{t^2+N-1}$ , with N being the number of subjects.

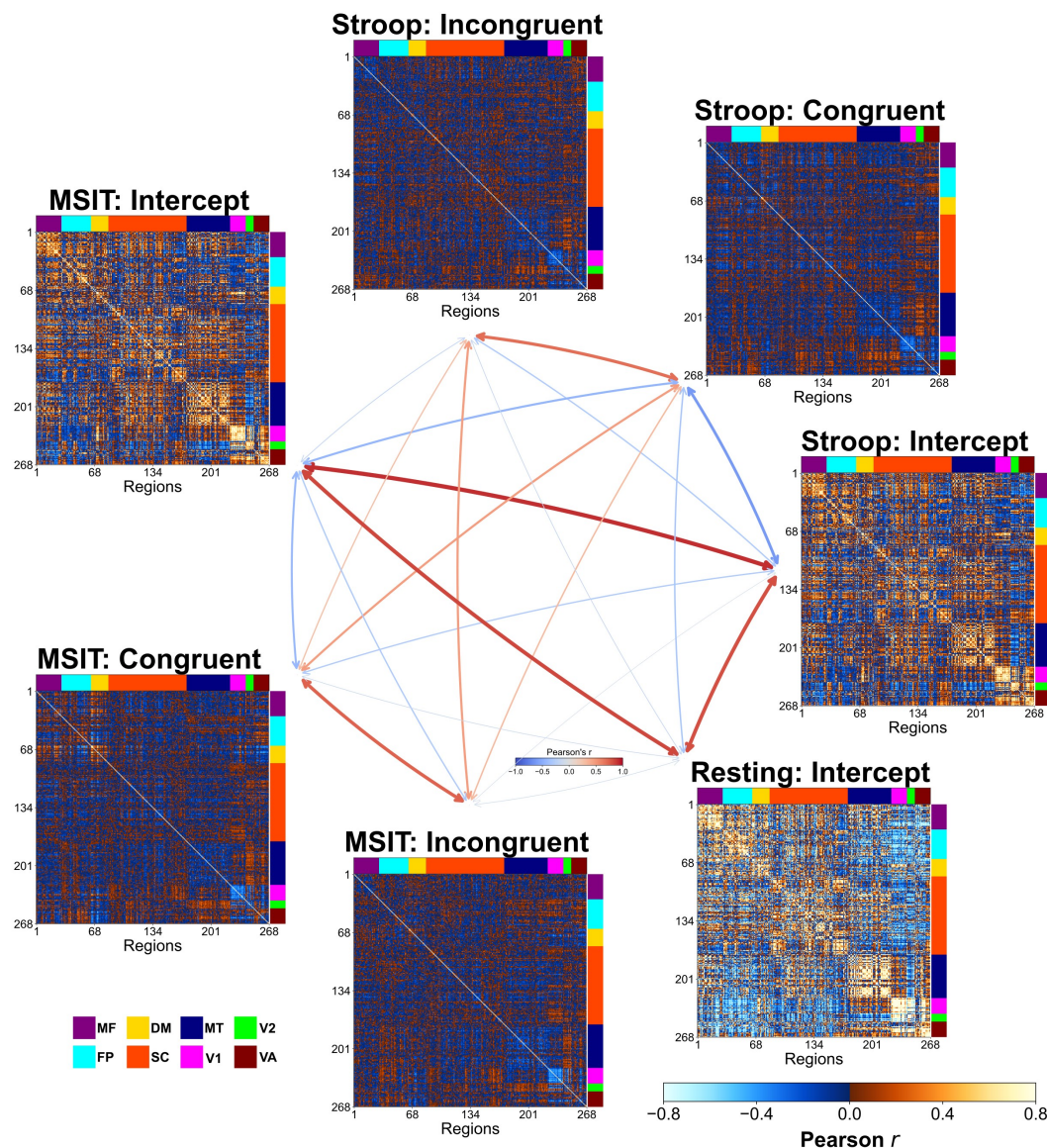
<sup>141</sup> The first thing to note is that, after accounting for condition effects during the two tasks, we were able  
<sup>142</sup> to recover the intrinsic brain networks observed during resting state. The intercept profiles for both  
<sup>143</sup> Stroop and MSIT had a high degree of similarity to the resting state profile ( $r = 0.85$  and  $r = 0.86$   
<sup>144</sup> respectively), as well as a high degree of similarity to each other ( $r = 0.94$ ).

<sup>145</sup> On the other hand, a largely different profile emerged during congruent and incongruent conditions in  
<sup>146</sup> both tasks. These networks showed much lower overall functional correlations, and a shift towards more  
<sup>147</sup> negative correlations, than the intercept profiles. Despite this difference from the intrinsic networks, the  
<sup>148</sup> condition-related profiles (i.e. congruent and incongruent) had a decent degree of within-task similarity  
<sup>149</sup> ( $r = 0.72$  for Stroop and  $r = 0.75$  for MSIT), demonstrating that both conditions recruit largely  
<sup>150</sup> consistent networks overall. Less similarity was observed between-task profiles, whether it be using  
<sup>151</sup> within-condition comparisons ( $r = 0.54$  for congruent;  $r = 0.83$  for incongruent), or between-condition  
<sup>152</sup> comparisons (Stroop congruent-MSIT incongruent  $r = 0.39$ , Stroop incongruent and MSIT congruent  
<sup>153</sup>  $r = 0.31$ ).

<sup>154</sup> Taken together, these results confirm that our method was able to reliably characterize both task and  
<sup>155</sup> intrinsic (resting) networks, at the group level, using the edge time series.

<sup>156</sup> ***Network profile differences between task conditions***

<sup>157</sup> The network profiles that emerged as a consequence of conflict processing were quantified at the group  
<sup>158</sup> level by contrasting subject-level functional correlations from both task conditions. The resulting  
<sup>159</sup> incongruent-vs-congruent statistical maps for both tasks are displayed in Fig. 4 (left plots, panels A and



136 **Figure 3. Functional correlation matrices at the group level.** For Stroop task, MSIT and resting-state functional correlation matrices using the intercept,  
137 congruent, and incongruent GLM estimations at the group level. Regions (i.e. the rows and columns) have been arranged based on their belonging to a major  
138 intrinsic network system (see Methods). In the middle in the form of a graph, the Pearson's correlation coefficients between the upper-triangular elements  
139 of these matrices. MF: Medial-Frontal; FP: Frontoparietal; DM: Default-mode; SC: Subcortical-Cerebellum; MT: Motor; V1: Visual-1; V2: Visual-2; VA:  
140 Visual-Association.

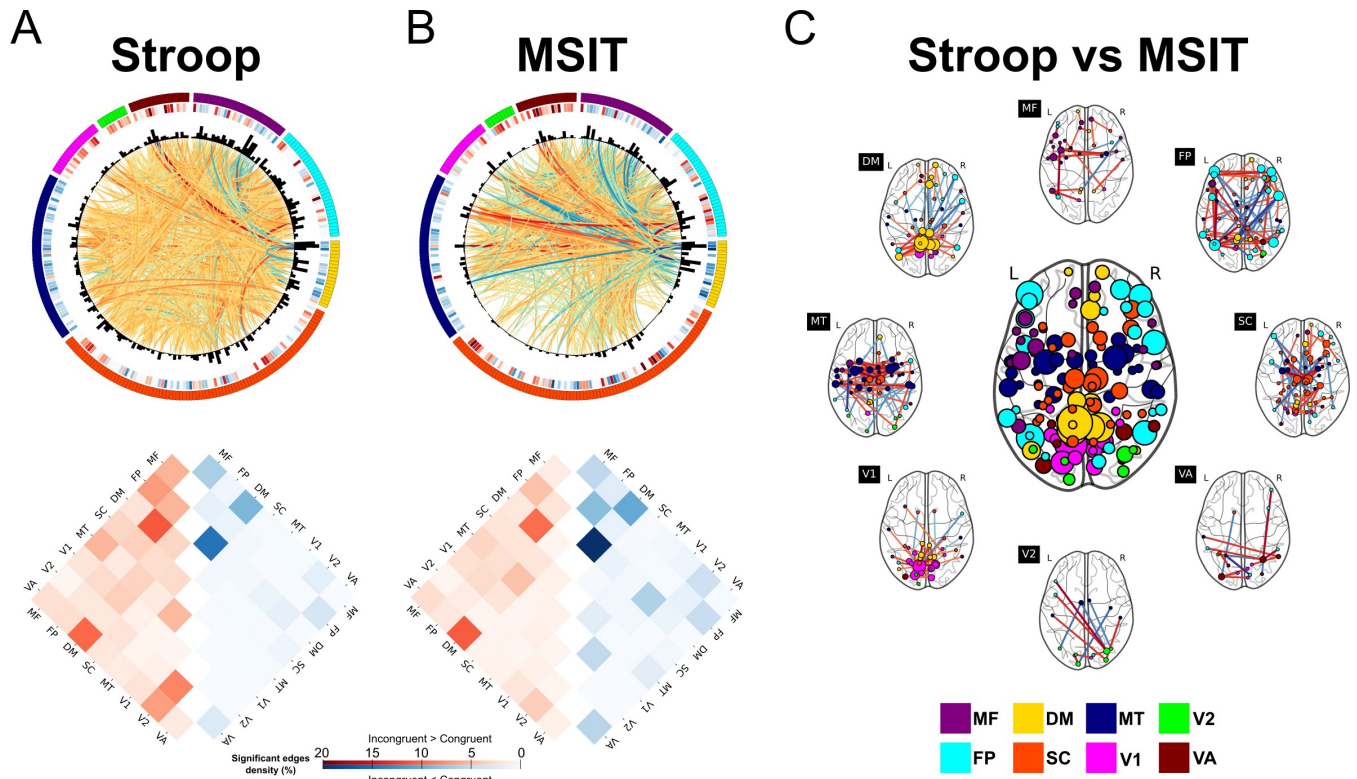
160 B), with 1284 (Stroop task) and 1042 (MSIT) edges that were significant at  $\alpha = 0.05$  after family-wise  
161 (Holm-Bonferroni procedure) error correction (red colors denote greater functional correlations during

162 incongruent trials than during congruent trials, and blue colors the opposite). In both cases, network  
 163 differences were primarily associated with default-mode, frontoparietal, medial-frontal, and visual  
 164 systems, as measured by the average significant edges per region found in those networks. Furthermore,  
 165 inspecting the sign of these differences (Fig. 4, right side of panels A and B), increased functional  
 166 correlations appeared to be dominated by edges connecting regions of distinct intrinsic major systems,  
 167 particularly those between the default-mode and the frontoparietal and visual-association systems, and  
 168 medial-frontal areas with the frontoparietal cortex. In contrast, significant decreases in functional  
 169 correlations during incongruent trials appeared in regions of the same major system, especially those  
 170 within the default-mode and medial frontal networks.

179 However, despite the apparent qualitative similarity in network-level responses to congruent and  
 180 incongruent conditions, the Stroop and MSIT also exhibited key differences. For example, concentrating  
 181 on the 10% of edges with the largest absolute t-stat values ( $n=358$ ), the Stroop task contained a  
 182 significantly greater number of positive (i.e. increased functional correlation during incongruent trials) to  
 183 negative (i.e. decreased functional correlation during incongruent trials) edges than the MSIT (Fisher  
 184 exact's test, odds ratio = 4.10,  $p = 1.17 \times 10^{-14}$ ). On the other hand, a paired-sample t-test performed on  
 185 individual edges revealed that these between-task network differences spanned the entire brain (see Fig.  
 186 4C), though they prominently expressed in the dorsolateral prefrontal and posterior parietal cortex, both  
 187 responsible for executive function, as well as in the posterior cingulate cortex, that is strongly implicated  
 188 during control processes, and the primary visual cortex. As a consequence, these results suggest that the  
 189 Stroop task and MSIT have substantial differences in their network profiles.

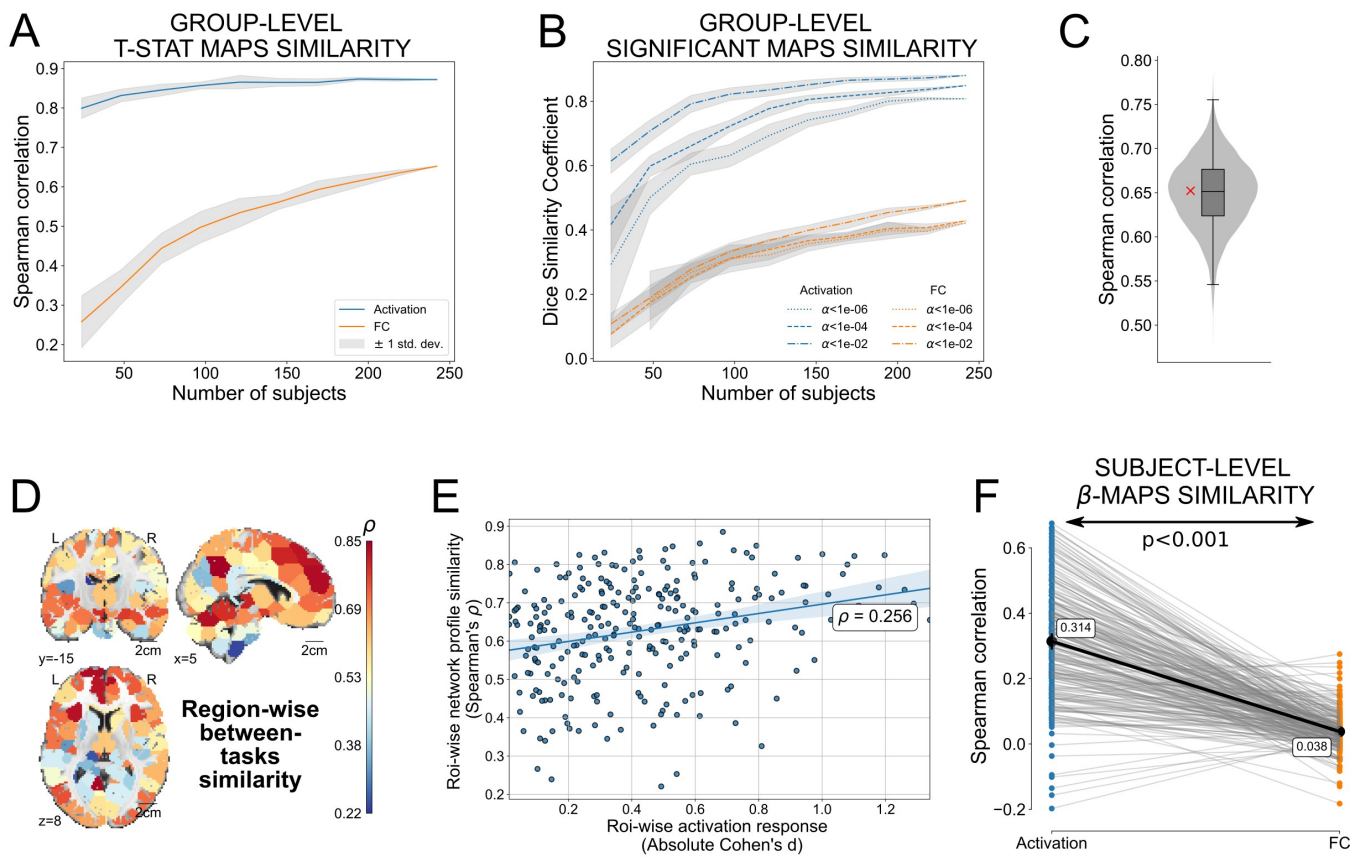
190 ***Comparison of similarities in activation patterns and network profiles between tasks***

191 We have previously shown that both Stroop and MSIT elicit largely overlapping patterns of brain  
 192 activation ( $\rho = 0.87$ ,  $DSC = 0.85$ ; see also Sheu et al. (2012)). In contrast, estimated edge-wise  
 193 responses suggest that both tasks appeared to differ at the network level. Is the lower similarity of  
 194 network profiles between-task really that different than the similarity in activation patterns? The  
 195 between-task similarity in incongruent-vs-congruent network profiles was equal to  $\rho = 0.65$  and  
 196  $DSC = 0.42$  at  $\alpha = 0.05$ , after family-wise (Holm-Bonferroni) correction, which indeed constitutes a  
 197 considerable reduction with respect to the aforementioned similarity rates from activation patterns.



171 **Figure 4. Group-level incongruent-vs-congruent functional correlation differences.** For Stroop task (A) and MSIT (B), on the top side and from outer  
 172 to inner circular, plots display each region arranged and colored according to the major functional system, their incongruent-vs-congruent activity at the node  
 173 level, their degree from the incongruent-vs-congruent significant edges, and finally the t-stat of these edges (red: incongruent > congruent, blue: incongruent <  
 174 congruent). At both node and edge levels, only significant results (at  $\alpha = 0.05$ , Bonferroni corrected) are shown. On the bottom side the number of significant  
 175 edges within and between major functional connectivity networks, normalized by the total number of edges in each case. (C) Using the significant edges  
 176 from a paired t-test at  $\alpha = 0.05$  (false-discovery rate corrected), between-task differences in incongruent-vs-congruent functional correlations shown in region  
 177 degree (inner brain plot), and with the edge t-stats to regions of each major functional system (outer brain plots). MF: Medial-Frontal; FP: Frontoparietal; DM:  
 178 Default-mode; SC: Subcortical-Cerebellum; MT: Motor; V1: Visual-1; V2: Visual-2; VA: Visual-Association.

198 Furthermore, this reduction became even more evident as the number of subjects decreased (Fig. 5A),  
 199 suggesting that this does not reflect an issue with statistical power in our sample. Also, this effect is  
 200 largely insensitive to using Spearman's  $\rho$  as a similarity measure since the same effect was observed  
 201 using Dice similarity coefficients at different thresholds (see Fig. 5B).



202 **Figure 5. Between-task similarity of activation patterns and network profiles.** A) Spearman's correlations between tasks from the group-level t-stat  
 203 incongruent-vs-congruent maps for both brain activation (blue line) and task-based functional correlations (FC, orange line), varying the number of subjects  
 204 used for their estimation. Each curve represents the average similarity and the gray area is the standard deviation after repeating 10 times the estimation  
 205 procedure to consider different subjects. B) Same as A) but using the dice similarity coefficient. Statistical maps were binarized according to whether each  
 206 t-stat was significant or not under several thresholds  $\alpha$ . C) Distribution of Spearman's correlations  $\rho$  between MSIT and Stroop functional correlation profiles  
 207 from 10000 subsamples that each randomly selected a subset of edges equal to the number of regions (268). The red cross displays the correlation using the  
 208 full profiles (i.e. 35778 edges). D) Region-wise similarity between tasks, using the whole-brain incongruent-vs-congruent network profile of each region. E)  
 209 These similarity rates per region (y-axis) are plotted versus their activation levels, measured as the average of both tasks' incongruent-vs-congruent absolute  
 210 Cohen's d at the group level. F) For each subject (a dot in the figure), the Spearman's correlation between the incongruent-vs-congruent  $\beta$  map of each task for  
 211 both brain activation (blue points) and task-based functional correlations (orange points). A paired t-test then quantified the statistical difference between both  
 212 distributions.

213 In order to show that this reduction in similarity scores between the incongruent-vs-congruent  
 214 functional correlation graphs was not due to correlating a larger number of features from the edges  
 215 ( $\frac{268 \times 267}{2} = 35778$  edges) than in the activation maps (only 268 components, since these were also  
 216 considered at the region-level), we repeated this calculation taking subsamples (number of  
 217 subsamples=10000) that randomly selected 268 edges in the functional correlation profiles. Across all  
 218 subsets, we found similar between-task Spearman's correlation values ( $0.65 \pm 0.04$ , see Fig. 5C) as the  
 219 one using the full network.

220 Along similar lines, we explored how the similarity of network profiles was expressed across the brain  
 221 by correlating, for each region, the whole-brain incongruent-vs-congruent functional correlation profile  
 222 (a vector of 267 t-stat values, i.e, we do not consider the diagonal terms in the functional correlation  
 223 profiles) at the group level of both tasks (see Fig. 5D). This analysis showed that there are certain regions,  
 224 particularly in the superior medial and dorsolateral-frontal gyrus, the precuneus, and the anterior lobe of  
 225 the cerebellum, that exhibit comparable, and sometimes even greater, similarity values than that from  
 226 activation patterns. While regions with the largest between-task similarities in activation did tend to have  
 227 higher degrees of between-task similarity in network profiles (Fig. 5E), this association was fairly weak  
 228 ( $\rho = 0.256$ ), suggesting that our main conclusion would also be reached if one focused exclusively on the  
 229 sub-network typically engaged during both Stroop and MSIT.

230 Since the previous calculation concentrated exclusively on group-level patterns, we also tested whether  
 231 the same qualitative findings were present at the within-subject level. Specifically, for each individual we  
 232 correlated, between tasks, the incongruent-vs-congruent activation maps and functional correlation  
 233 graphs, using in both cases the  $\beta$  estimations (see the sample distributions in Fig. 5F). The reason for  
 234 using the  $\beta$  estimations here instead of the t-stat values is that temporal autocorrelations in the time series  
 235 produced a different number of degrees of freedom across nodes and edges in both tasks, in contrast to  
 236 the group level, where the degrees of freedom always remained the same ( $N - 1$ , with  $N$  the number of  
 237 subjects). A paired t-test showed that, as found before with the group-level maps, between-task similarity  
 238 rates of brain activation maps ( $< \rho > = 0.314$ , 95% CI [0.292, 0.335]) were higher than those from  
 239 task-based network differences ( $< \rho > = 0.038$ , 95% CI [0.031, 0.045]; Cohen's  $d = 1.584$ ,  $p < 0.001$ ).

240 The preceding analysis shows how two tasks with similar activation patterns may not have as similar  
 241 network profiles. One likely explanation for this could be that the correlation ceiling for the former

measure (activation) is simply higher than the ceiling for the latter (connectivity), but two individuals more similar in activation patterns may also be more similar in their functional network architecture. In order to rule this out, we conducted, for each task separately, a Mantel test on the upper triangular terms of the distance matrices  $d_{ij}^{act}$  and  $d_{ij}^{conn}$ . This directly tests whether similarity in activation patterns correlates with similarity in network profile at the pairwise subject level. For consistency with the previous analyses, we adopted a Spearman's correlation-based metric, i.e.  $d_{ij} = 1 - \rho_{ij}$ , for defining the distance between any pair of subjects  $i$  and  $j$ . We found that these two matrices were not significantly correlated in either of the two tasks (Stroop:  $r = 0.005$ , 95% CI [-0.123, 0.159]; MSIT:  $r = 0.072$ , 95% CI [-0.055, 0.204]). Confidence intervals were calculated using 100,000 resamples without replacement and a subsampling ratio of 0.135, following the indications in Balakrishnan, Choe, Singh, Vettel, and Verstynen (2018). These results suggest that the observed difference in similarity rates between activation patterns and network profiles exists beyond any ceiling effect and is persistent even in within-subject comparisons.

We ran several follow-up tests to examine the robustness of all these findings with respect to changes in the analytical pipeline. First, we investigated whether the reduction in between-task similarity in network profiles, compared with evoked responses, was not due to removing the task stimuli prior to calculating the edge time series. Supplementary Fig. 1A shows a mild increase at the subject level when tasks effects are maintained ( $<\rho> = 0.080$ , 95% CI [0.071, 0.088]) and it is still significantly lower with respect to activation patterns (Cohen's  $d = -1.535$ ,  $p < 0.001$ ). Moreover, a similar finding was observed (see Supplementary Fig. 1, panel B) when we concentrated exclusively on the regions with the greatest task activation responses (group-level incongruent-vs-congruent absolute Cohen's  $d$ 's larger than 0.8 in both tasks). Thus the choice of how we regress out task effects prior to building the edges-time series does not drive our primary effect of differences in similarity profiles between activation and network profiles.

Subsequently, we tested whether including in our parcellation specific brain structures that are known to be noisier or more susceptible to signal loss, namely the cerebellum and subcortex, might have driven our findings. In order to achieve this, we repeated the subject-level similarity analysis using a Craddock atlas (Craddock, James, Holtzheimer, Hu, & Mayberg, 2011), consisting of 200 regions that did not include the cerebellum, and the Schaefer atlas (Schaefer et al., 2017), comprising 200 cortical regions. Additionally, we considered a combination of 10 ICA-based major areas from Smith et al. (2009), and 7

271 bilateral subcortical regions from the Harvard-Oxford atlas (thalamus, caudate, putamen, pallidum,  
 272 hippocampus, amygdala and accumbens). This customized atlas was included to intentionally test a  
 273 parcellation that yields a smaller number of edges than the number of nodes in the Shen atlas (268  
 274 regions). We found, again, that the choice to use the Shen atlas was not decisive in our primary effect of  
 275 the differences between activation and network profile similarities (see Supplementary Fig. 1, panel C).

276 Likewise, we wondered whether the reduction in similarity between Stroop and MSIT task-dependent  
 277 network profiles was influenced by the edge time series approach itself. We tested this possibility by  
 278 replicating our analyses using a generalized Psychophysiological Interaction (PPI) model, which is a  
 279 standard and common framework for assessing task-modulated functional connectivity (see Materials &  
 280 Methods for details on this model). As Supplementary Fig. 1D illustrates, these PPI-based network  
 281 profiles also showed a reduced similarity between tasks ( $\rho = 0.550$ ,  $DSC = 0.357$  at  $\alpha = 0.05$  after  
 282 family-wise error correction) compared to what is observed in the brain activation patterns. In addition,  
 283 albeit small differences existed, particularly within the motor system, both approaches (edge time series  
 284 and PPI) appeared to yield fairly similar incongruent-vs-congruent contrast network profiles in both tasks  
 285 ( $\rho = 0.743$  for Stroop,  $\rho = 0.786$  for MSIT).

286 A compact summary of the between-task activation and network profile similarity values covering  
 287 debatable methodological choices can be found in Supplementary Fig. 2. These comprised how  
 288 aggressively task stimuli were removed before computing the edge time series, the hemodynamic  
 289 response function model, whether global signal regression was performed, whether time series at the  
 290 node and edge level were standardized in the GLM, and whether prewhitening was applied. We can see  
 291 that our findings at both the group and single-subject levels were consistent across all the different  
 292 methodological setups. This notably included global signal regression, a step that is still controversial in  
 293 task-effect estimations (Liu, Nalci, & Falahpour, 2017).

294 Finally, one may argue that the observed differences in between-task similarity degrees are simply a  
 295 consequence of functional connectivity being inherently noisier than activation measures. Indeed, the  
 296 signal-to-noise ratio (SNR), defined for our contrast-of-interest as  $SNR = \left( \frac{|\beta_{inc} - \beta_{con}|}{\sigma_{(inc-con)}} \right)$  and calculated as  
 297 the median value across nodes/edges, is weak for connectivity (group-level  $SNR_{stroop} = 0.09$ ,  
 298  $SNR_{msit} = 0.081$ ) and small-to-medium for activation (group-level  $SNR_{stroop} = 0.38$ ,  $SNR_{msit} = 0.406$ ).  
 299 As a consequence, we reran our analysis concentrating exclusively on those nodes and edges with at least

300 a medium SNR at the group level in both tasks ( $\text{SNR} > 0.5$ ). We found that even in this (stringent)  
 301 scenario with balanced signal-to-noise ranges there remain substantial differences in between-task  
 302 similarity values at both the group (activation:  $\rho = 0.911$ , connectivity:  $\rho = 0.775$ ) and subject level  
 303 (activation:  $<\rho> = 0.547$ , 95% CI [0.524, 0.574], connectivity:  $<\rho> = 0.301$ , 95% CI [0.27, 0.333];  
 304 activation vs connectivity Cohen's  $d = 0.819$ ,  $p < 0.001$ ). Thus, signal-to-noise does not appear to be a  
 305 mediating factor in this effect.

## DISCUSSION

306 Here we set out to validate previous computational modeling work showing that similarity in patterns of  
 307 activation do not imply similarity in underlying network states (Goldman, Golowasch, Marder, & Abbott,  
 308 2001; Golowasch, Abbott, & Marder, 1999; Prinz et al., 2004; Roffman, Norris, & Calabrese, 2012).  
 309 Using a GLM framework on instantaneous functional correlation estimates (Faskowitz, Esfahlani, Jo,  
 310 Sporns, & Betzel, 2020; Zamani Esfahlani et al., 2020), we were able to successfully separate task-free  
 311 (intrinsic) from task-dependent network contributions, in line with the extensive evidence that task  
 312 functional correlations are jointly shaped by both intrinsic and evoked network architectures (Cole,  
 313 Bassett, Power, Braver, & Petersen, 2014). Subsequently, we showed how our two tasks shared a large  
 314 degree of similarity in activation topology (nodes), but substantially less similarity in network profiles  
 315 (edges). This difference in task effects at the nodes and edges was confirmed at both group and subject  
 316 levels, and using two different measures commonly employed for representational similarity analyses.  
 317 Likewise, this difference between activation and network profiles was replicated after keeping task effects  
 318 in the edge time series, employing different parcellations, using a different method for estimating  
 319 task-related functional connectivity (i.e., PPI), exploring a wide array of methodological choices (e.g.  
 320 including or excluding the brain global signal as a covariate), and balancing signal-to-noise differences.  
 321 Taken together, these results highlight how similarity in activation does not necessarily imply similarity  
 322 in underlying network profile, reflecting the fact that the underlying cognitive processes manifest at both  
 323 the node (voxel or region) and edge (connectivity) levels.

324 As pointed out by Prinz and colleagues (2004), the multiple realizability problem of many network  
 325 states leading to the same activation pattern poses a challenge when interpreting subject-to-subject  
 326 differences (Prinz et al., 2004) (see also Krakauer, Ghazanfar, Gomez-Marin, MacIver, and Poeppel

327 (2017)). Indeed, over the past 10 years there has been both increased interest in, and increased pushback  
 328 against, using task-related fMRI as a means of predicting individual differences in healthy (Gianaros et  
 329 al., 2020, 2022; Greene, Gao, Scheinost, & Constable, 2018; Jiang et al., 2020; Rosenberg et al., 2015;  
 330 Tetereva, Li, Deng, Stringaris, & Pat, 2022; Wager et al., 2013) and pathological populations (Andersen,  
 331 Rayens, Liu, & Smith, 2012; Costafreda et al., 2011; Hart et al., 2014; Just, Cherkassky, Buchweitz,  
 332 Keller, & Mitchell, 2014; Koch et al., 2015; Mourão-Miranda et al., 2011; Yoon et al., 2012). A  
 333 fundamental assumption of the statistical tools used in these studies is that if two people are similar in  
 334 their brain activation they will also be similar in the outcome measure being predicted. Our results show  
 335 how this fundamental assumption may not always hold: two people may produce the same pattern of  
 336 task-related activation, but rely on fundamentally different network-level representations. Indeed, this  
 337 may help to explain why the effect sizes of brain phenotype studies are so low compared to what would  
 338 be needed to produce medical-grade diagnostic tools (Marek et al., 2022).

339 It is worth pointing out that while network profiles do differ more between tasks than activation  
 340 patterns, we still observed a modest degree of similarity in network profiles across tasks. This is not  
 341 surprising given the existence of a core functional architecture shared between even markedly different  
 342 task states (Krienen et al., 2014). In our case, the greatest similarities were found in networks that are  
 343 reliably associated with sensory processing and motor planning. While motor planning constraints were  
 344 identical across tasks (i.e., both involved button presses with the same hand and fingers), the visual  
 345 stimuli were quite different (see Fig. 6). This suggests that the between-task dissimilarities in network  
 346 profiles reflect differences in *how* sensory information is used during action selection, after sensory  
 347 representations are formed, rather than simple bottom-up effects driven by the stimulus differences  
 348 between the Stroop task and MSIT. Adding to the other between-task topological differences that we  
 349 observed, involving mainly regions of the default-mode and executive networks, this appears to suggest  
 350 that greater deviations take place in subnetworks largely associated with higher-level cognitive functions.

351 One natural follow-up question is how the edge time series responses compare to other approaches for  
 352 addressing task-based networks like PPI. We have shown that, even though PPI arrives at the same  
 353 conclusion as the edge time series method, the network profiles obtained from both approaches were not  
 354 perfectly identical. While the edge time series straightforwardly represents measures of (instantaneous)  
 355 functional correlations, PPI was designed to assess effective connectivity (K. Friston et al., 1997;

356 K. J. Friston, 2011). Thus, in order to enable the comparison between both approaches in our study, PPI  
 357 estimates were symmetrized, so we speculate that part of these differences may come from this operation.  
 358 A full comparison with other common methods for task-related networks, such as correlational PPI  
 359 (Fornito, Harrison, Zalesky, & Simons, 2012) or beta series correlations (Rissman, Gazzaley, &  
 360 D'Esposito, 2004), could yield both interesting differences and show areas of robustness in network  
 361 profiles. However, this is well beyond the scope of the current project.

362 While our findings here provide strong evidence in support of the idea that similarity in activation does  
 363 not imply similarity in network state, it is worth noting some significant limitations. First, all our  
 364 analyses have been performed at the macroscopic level. As mentioned above, even though evidence  
 365 suggests that a similar behavior is expected at smaller network scales, future studies should test this *ex*  
 366 *profeso*. On a related point, since the correlation matrices become computationally intractable at the  
 367 voxel level, and in order to maintain both activation and network measures with the same spatial  
 368 resolution, we opted to perform all analyses at the region level, using a predefined parcellation template.  
 369 This obviously introduces some degree of anatomically bounded spatial smoothing in the data, which  
 370 may be contributing to inflating the similarities in both task-related activation and network profiles  
 371 between tasks. Smoothing would be problematic if we were interested in null hypothesis tests on spatial  
 372 patterns (Markello & Misic, 2021), however, the analysis used here does not rely on such spatial  
 373 hypothesis testing. Thus, this region-level approach does not invalidate the main conclusions of our study  
 374 that similarity in the topology of activation patterns does not perfectly associate with similarity in  
 375 network architecture.

376 Finally, one might question whether the BOLD time series first needed to be deconvolved with the  
 377 hemodynamic response function prior to estimating the edge time series. It has been argued that  
 378 deconvolution in block-design tasks, like our Stroop task and MSIT, may not be necessary (Di & Biswal,  
 379 2017; Di, Zhang, & Biswal, 2020). However, it is important to point out that while changing the choices  
 380 in the preprocessing and analysis steps may lead to nuanced differences in certain aspects of our results,  
 381 none of these potential limitations would likely change the primary conclusion we have drawn from our  
 382 observations.

383 Regardless of these limitations, our results clearly illustrate that important aspects of task  
 384 representations are encoded in the associations between regions, which are unique to and complement

385 information reflected in the spatial topology of activation (Chan et al., 2017; Gratton et al., 2016).  
 386 Indeed, our findings bolster previous work looking at informational connectivity (Coutanche &  
 387 Thompson-Schill, 2013), which highlights the information value of associations between regions in  
 388 understanding task representations. This poses significant challenges for interpreting individual  
 389 differences based on activation patterns alone. Further work should dig deeper into the high-dimensional  
 390 relationships between localized activation and global connectivity dynamics when trying to understand  
 391 the nature of representations in the brain.

## MATERIALS AND METHODS

### *392 Participants*

393 We analyzed task and resting-state fMRI data from the Pittsburgh Imaging Project (PIP), which is a  
 394 registry of behavioral, biological, and neural correlates of cardiovascular disease risk among otherwise  
 395 healthy community-dwelling adults (aged 30–54 years). Details of this project can be found in the  
 396 supplementary material of Gianaros et al. (2020). We selected a subset of 242 subjects (female=119,  
 397 mean age=40 ± 6 years, min age=30 years, max age=51 years) that had full temporal and spatial  
 398 coverage and exhibited low average motion (mean framewise displacement, estimated using the method  
 399 in Power, Barnes, Snyder, Schlaggar, and Petersen (2012), lower than 0.35 mm) across the three fMRI  
 400 acquisitions used in our study.

### *401 MRI Data Acquisition*

402 MRI data were acquired on a 3 Tesla Trio TIM whole-body scanner (Siemens, Erlangen, Germany),  
 403 equipped with a 12-channel head coil. Functional blood-oxygen-level-dependent (BOLD) images were  
 404 acquired from a T2\*-weighted gradient echo-planar imaging sequence (repetition time=2000 ms, echo  
 405 time=28 ms; field of view=205 × 205 mm (matrix size=64 × 64), slice thickness=3 mm (no gap); and flip  
 406 angle=90°). For anatomical coregistration of the fMRI images, a high-resolution T1-weighted image per  
 407 subject was also acquired (MPRAGE, repetition time = 2100 ms, echo time=3.29 ms, inversion  
 408 time=1100 ms, flip angle=8°, field of view=256 mm × 208 mm (matrix size: 256 × 208), slice  
 409 thickness=1 mm with no gap).

### *410 Tasks*

<sup>411</sup> We used two tasks that involved processing conflicting information and response inhibition. Both tasks  
<sup>412</sup> consisted of 4 blocks that defined a congruent information condition, interleaved with 4 blocks of trials  
<sup>413</sup> where the participant received incongruent information. Both task conditions had a duration of 52-60  
<sup>414</sup> secs and were preceded by a variable 10-17 sec fixation block. In total, each task had a duration of 9 min  
<sup>415</sup> and 20 secs.

<sup>416</sup> In the color-word Stroop task, participants had to select 1 of 4 identifier words using a response glove  
<sup>417</sup> (e.g., thumb button 1 = identifier word on the far left, etc.), such that its name indicates the color of target  
<sup>418</sup> words located in the center of a screen. During the congruent trials, the four identifier words were all in  
<sup>419</sup> the same color as the target words. Instead, in incongruent trials, identifier words had all different colors,  
<sup>420</sup> and the option to select was in a color incongruent with the target words. This kind of task usually evokes  
<sup>421</sup> a brain response that activates regions in the anterior insula, parietal cortex, basal ganglia, thalamus, and  
<sup>422</sup> cerebellum; while deactivating areas that belong to the so-called ‘default-mode network’ (see Fig. 6A, B  
<sup>423</sup> and C).

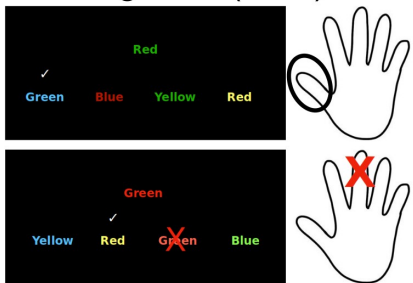
<sup>427</sup> In the MSIT, which corresponded here to a modification from the original task version (Bush & Shin,  
<sup>428</sup> 2006), participants had to select 1 of 3 numbers such that it differed from the other 2 by pressing buttons  
<sup>429</sup> on the glove, where each button matched a number on the screen (thumb button 1 = number 1, etc.).  
<sup>430</sup> During congruent trials, the targets’ position matched that on the glove, whereas during incongruent trials  
<sup>431</sup> this position did not match the glove’s button location. This task elicits a brain pattern response that is  
<sup>432</sup> largely similar to that in the Stroop task (see Fig. 6D, E and F and Sheu et al. (2012) for more details on  
<sup>433</sup> the MSIT and the Stroop task).

<sup>434</sup> In incongruent conditions of *both* tasks, accuracy was titrated to ~ 60% by altering intertrial intervals,  
<sup>435</sup> i.e. consecutive accurate choices led to shortened intertrial intervals. To control for motor response  
<sup>436</sup> differences between conditions in both tasks, the number of trials in the congruent condition was yoked  
<sup>437</sup> to the number completed in the incongruent condition. Yoking was implemented by (1) administering an  
<sup>438</sup> incongruent block first and (2) presenting congruent condition trials at the mean intertrial interval of the  
<sup>439</sup> preceding incongruent block.

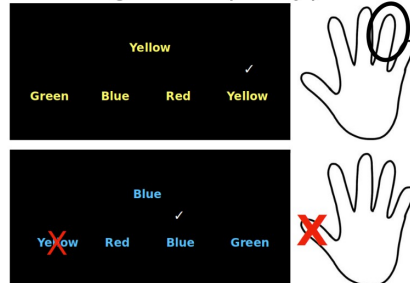
<sup>440</sup> Finally, we also used a five-minute resting-state scan, during which the participants were told to keep  
<sup>441</sup> their eyes open.

## Color-Word Stroop Task

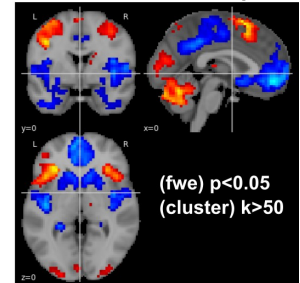
**A Incongruent (hard) trial**



**B Congruent (easy) trial**

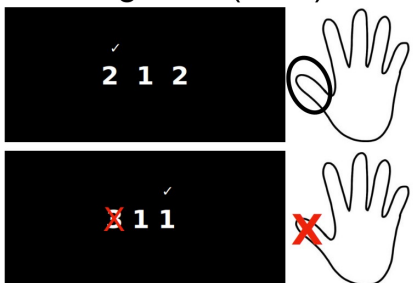


**C T-stat contrast map**

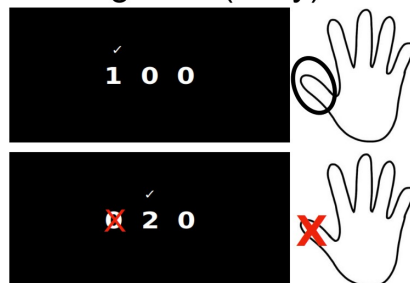


## Multisource Interference Task (MSIT)

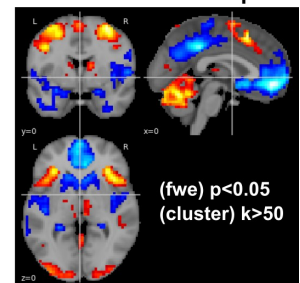
**D Incongruent (hard) trial**



**E Congruent (easy) trial**



**F T-stat contrast map**



424 **Figure 6. Stroop task and MSIT paradigms and their brain response.** For both Stroop task and MSIT, illustration of incongruent (A, D) and congruent  
425 trials (B, E). Trials consisted of blocks of 52–60 s duration, interleaved with a 10–17 s fixation block. Contrasting brain activity between incongruent and  
426 congruent conditions gives rise to a similar brain response (C, F).

### 442 **Preprocessing**

443 Data were preprocessed using fMRIprep (Esteban et al., 2018), a standard toolbox for fMRI data  
444 preprocessing that provides stability to variations in scan acquisition protocols, a minimal user  
445 manipulation, and easily interpretable, comprehensive output results reporting. First, anatomical data  
446 preprocessing was performed, including bias-field correction, skull-stripping, brain extraction and tissue  
447 segmentation, and surface reconstruction. It was then followed by functional data preprocessing, which  
448 included reference image estimation, head-motion parameters estimation, slice time correction,  
449 susceptibility distortion correction via a nonlinear registration (“Fieldmap-less” option of the toolbox),  
450 spatial normalization and confounds estimation.

451 ***Functional Correlation (Edge) analysis***

452 We estimated task-based functional correlations using the edge, or co-fluctuation, time series proposed in  
 453 (Faskowitz et al., 2020; Zamani Esfahlani et al., 2020). One of the advantages of using this edge time  
 454 series measure is that the procedure for estimating patterns of task-based functional correlation is by  
 455 nature the same as that in GLM-based activation analyses but simply changing the outcome variable. A  
 456 sketch of this full estimation procedure can be found in Fig. 7. We first (step A) reduced the spatial  
 457 resolution of the preprocessed time series by computing the voxel-wise average signal within each region  
 458 (ROI) in a 268-parcel atlas (Shen, Tokoglu, Papademetris, & Constable, 2013). Following Finn et al.  
 459 (2015), each of these regions was also identified to a specific intrinsic functional connectivity network:  
 460 Motor, Visual-1, Visual-2, Visual-Association, Medial-Frontal, Frontoparietal, Default-mode and  
 461 Subcortical-Cerebellum. Then, let  $\vec{x}_i \equiv \{x_i(1), \dots, x_i(T)\}$  be the time series of  $T$  scans (the full-scan  
 462 sequence) for a given parcel  $i$  in such atlas. Each of these parcellated time series were subsequently (step  
 463 B) denoised by means of a linear regression model, in a single step that prevents artifacts from being  
 464 reintroduced in the data (Lindquist, Geuter, Wager, & Caffo, 2019), in order to remove effects from  
 465 motion (24 parameters which included 3 translations, 3 rotations, their derivatives and the square of all  
 466 these terms), the average white-matter signal, the average CSF signal, the average brain signal, periodic  
 467 oscillations greater than 187 s (5 cosine terms) and task activations (24 terms). This last set of regressors  
 468 consisted of 12 finite impulse response (FIR) terms per task condition (congruent and incongruent) to  
 469 flexibly model a hemodynamic response function (HRF) of about 24s to external stimuli and that was  
 470 included so as to avoid systematic inflation of functional correlations produced by task activations (Cole  
 471 et al., 2019). The resulting denoised ROI time series were standardized (step C), i.e.  $\vec{z}_i = \frac{\vec{x}_i - \mu}{\sigma}$ , and then  
 472 used to generate the edge time series  $\vec{r}_{ij}$  (step D) as the component-wise product between pairs of  
 473 standardized time series, i.e.  $\vec{r}_{ij} = \{z_i(1) \cdot z_j(1), \dots, z_i(T) \cdot z_j(T)\}$ . At this point, if we summed these  
 474 components up and divided by  $T - 1$ , we would obtain the Pearson correlation coefficient that usually  
 475 represents the static functional connectivity between BOLD time series - that is, each edge time series  
 476 can be interpreted as a temporal decomposition of a functional connection (correlation) into its framewise  
 477 contributions. Instead, we continued working on these edge time series as response variables in a general  
 478 linear model (step E) in order to estimate intrinsic and task-dependent functional correlation profiles. To  
 479 this end, the input design matrix included an intercept term and a set of regressors for each task condition

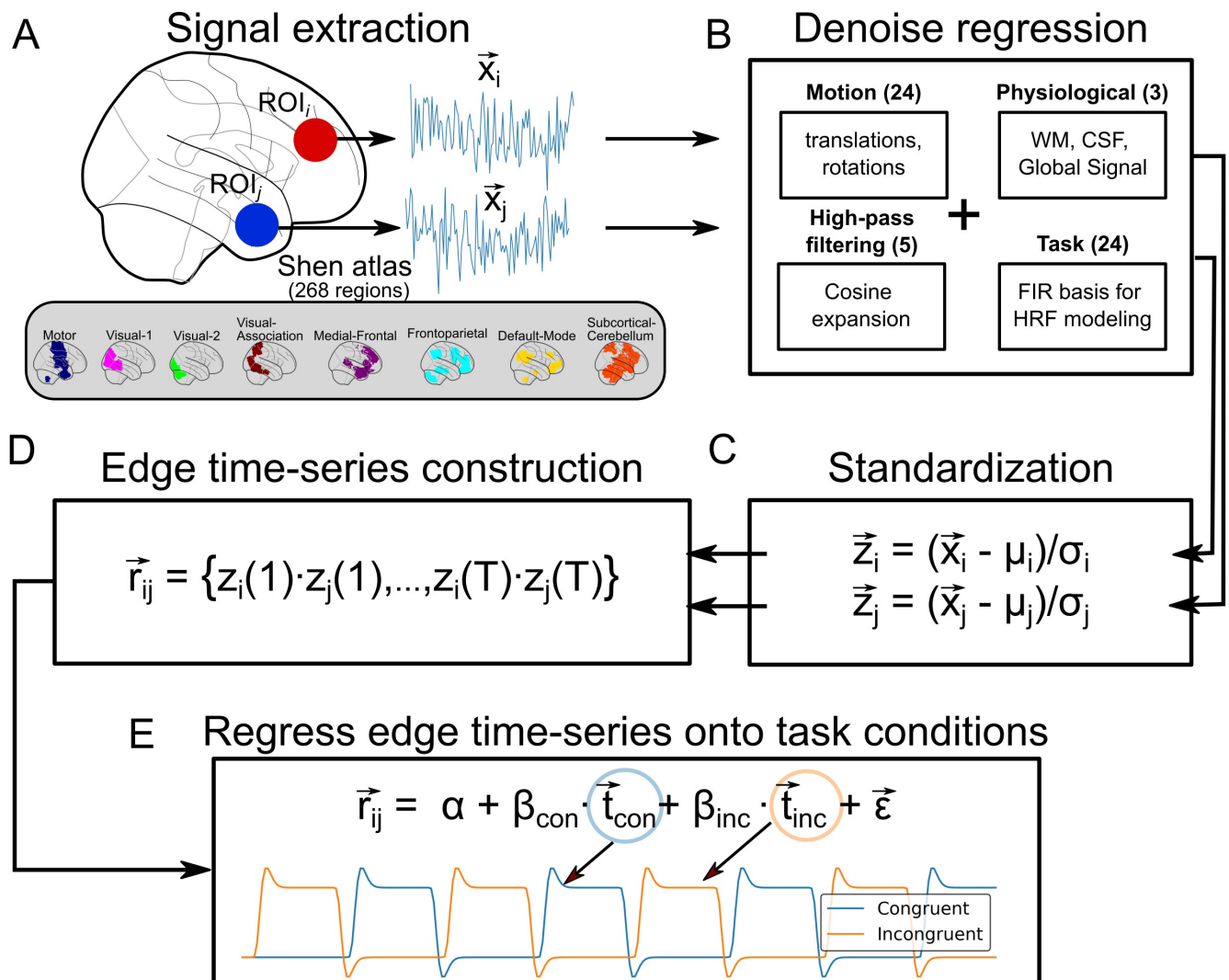
480 (congruent and incongruent), which comprised a boxcar function convolved with the usual double  
 481 gamma hemodynamic response function and its temporal and dispersion derivatives. Although it is not  
 482 clear that the usual hemodynamic response function also takes place in the edge time series, we decided  
 483 to assume it for pipeline compatibility with the activation (node) analysis (see next subsection).  
 484 Nevertheless, it is important to note that we repeated the same analytical pipeline considering just boxcar  
 485 regressors (i.e. without including the hemodynamic response convolution), and found no substantial  
 486 changes in the functional correlation profiles. Due to the considerable duration of each task condition, the  
 487 effects triggered by the convolution with the hemodynamic response function, which mainly happen at  
 488 the beginning and end of each task block, are dampened when averaging across all time points.

493 Prior to any statistical analysis, time series on both sides of the regression model were prewhitened  
 494 through a first-order autoregressive model in order to account for the temporal autocorrelations. As  
 495 aforementioned, we assumed this standard procedure for dealing with temporal autocorrelations in order  
 496 to have the same statistical pipeline as that in the activation analysis (see next subsection). Future studies  
 497 should investigate the most appropriate procedure for accounting for autocorrelations using edge time  
 498 series. After this first-level estimation, task-based network changes were computed as contrasts of  
 499 parameters and subsequently used to assess edge-wise group-level effects by means of a one-sample  
 500 t-test. Statistical inference at a usual 0.05 significance level was finally performed, after correcting the  
 501 family-wise error (Holm-Bonferroni procedure) due to multiple testing. All these statistical analyses of  
 502 the edge time series were carried out using Nilearn 0.7 (Abraham et al., 2014).

### 503 ***Activation (Node) analysis***

504 We also analyzed the preprocessed BOLD images at the node level, which involved estimating brain  
 505 activation changes during the different task conditions. Such analyses are usually carried out at the voxel  
 506 level. However, in order to keep the same resolution as that of the edge-level results, brain activations  
 507 were estimated at the region-level using the same parcellated BOLD time series.

508 For this analysis, we employed again a GLM with the parcellated BOLD time series as response  
 509 variables and a design matrix that included the same set of task regressors used in the edge-wise analyses,  
 510 as well as the same covariates that were regressed out prior to this, i.e. the 24 motion parameters  
 511 (K. J. Friston, Williams, Howard, Frackowiak, & Turner, 1996), the cosine terms to account for



489 **Figure 7. Estimation of intrinsic and task-related functional correlations.** For a given pair of regions in the Shen atlas (consisting of 268 regions),  
490 the average signal within them was first computed (A). The time series were then denoised (B) and standardized (C). Subsequently, they were multiplied  
491 component-wise (D). Finally, the resulting temporal profile was regressed onto a design matrix to model intrinsic (intercept term) and task-related functional  
492 correlations (E).

512 oscillation effects greater than 187s, the average signal within white-matter tissue, the average signal  
513 within CSF tissue, and the average signal within the whole brain. We considered this last regressor, not  
514 common in brain activation analyses, for consistency again with the edge-level analyses (see previous  
515 section). Group-level effects were similarly assessed using a one-sample t-test.

516 ***Generalized Psychophysiological Interaction***

As a part of our sanity check pipeline, we compared the functional correlation analysis using the aforementioned edge time series approach with a model of Generalized Psychophysiological Interactions (PPI), which is a standard approach for estimating task-dependent functional connectivity changes (McLaren, Ries, Xu, & Johnson, 2012) and is based on a general linear model of task-moderated temporal association between pairs of brain units. Specifically, for a given pair of BOLD time series  $\vec{x}_i$  and  $\vec{x}_j$ , such a model includes one of them as the response variable and as inputs the other BOLD time series, the group of task regressors, the interaction terms between these task regressors and the input BOLD time series, and the possible confounders to consider in the model. In our case, the generalized PPI model can be written as follows:

$$\vec{x}_i = \alpha + \beta_{ij}^{bck} \cdot \vec{x}_j + \beta^{task} \times \mathcal{T} + \beta_{ij}^{ppi} \times \mathcal{I}_i + \beta^{cov} \times \mathcal{C} + \vec{\epsilon}, \quad (1)$$

517 where  $\mathcal{T}$  is a matrix whose columns are the HRF convolved box-car congruent and incongruent time  
 518 profiles and their derivatives and dispersion terms,  $\mathcal{I}_i$  the matrix with the PPI terms from each condition,  
 519 i.e. the interaction term between each task condition's time profile and the input time series  $\vec{x}_i$ , and  $\mathcal{C}$  a  
 520 matrix with the different covariates to include in this model, which in our case comprised the 24 motion  
 521 parameters, the average white-matter signal, the average CSF signal, the average brain signal and cosine  
 522 expansion for a 187 sec high-pass filtering. Once all the parameters in this model were estimated,  
 523 task-based functional connectivity changes were evaluated by contrasting the incongruent and congruent  
 524 PPI estimations, and their effect at the group level was assessed using a one-sample t-test. In this way, a  
 525 matrix of estimated task-based functional connectivity changes can be constructed. However, since a PPI  
 526 model yields non-symmetrical matrices, we symmetrized them by averaging their corresponding upper  
 527 and lower triangular elements as done in Di, Reynolds, and Biswal (2017), which enabled direct  
 528 comparison with the functional connectivity profiles obtained from the edge time series approach.

## CODE AND DATA AVAILABILITY

529 The code used to generate all the analyses and results can be found in  
 530 <https://github.com/CoAxLab/cofluctuating-task-connectivity>.

531

532

533

## REFERENCES

- 534 Abraham, A., Pedregosa, F., Eickenberg, M., Gervais, P., Mueller, A., Kossaifi, J., ... Varoquaux, G. (2014). Machine  
 535 learning for neuroimaging with scikit-learn. *Frontiers in Neuroinformatics*, 8. Retrieved from  
 536 <https://doi.org/10.3389/fninf.2014.00014> doi: 10.3389/fninf.2014.00014
- 537 Alnæs, D., Kaufmann, T., Richard, G., Duff, E. P., Snee, M. H., Endestad, T., ... Westlye, L. T. (2015). Attentional load  
 538 modulates large-scale functional brain connectivity beyond the core attention networks. *NeuroImage*, 109, 260–272.  
 539 Retrieved from <https://doi.org/10.1016/j.neuroimage.2015.01.026> doi:  
 540 10.1016/j.neuroimage.2015.01.026
- 541 Anders, S., Lotze, M., Erb, M., Grodd, W., & Birbaumer, N. (2004). Brain activity underlying emotional valence and  
 542 arousal: A response-related fMRI study. *Human Brain Mapping*, 23(4), 200–209. Retrieved from  
 543 <https://doi.org/10.1002/hbm.20048> doi: 10.1002/hbm.20048
- 544 Andersen, A. H., Rayens, W. S., Liu, Y., & Smith, C. D. (2012). Partial least squares for discrimination in fMRI data.  
 545 *Magnetic Resonance Imaging*, 30(3), 446–452. Retrieved from  
 546 <https://doi.org/10.1016/j.mri.2011.11.001> doi: 10.1016/j.mri.2011.11.001
- 547 Balakrishnan, S., Choe, Y., Singh, A., Vettel, J. M., & Verstynen, T. D. (2018). Local white matter architecture defines  
 548 functional brain dynamics. *2018 IEEE International Conference on Systems, Man, and Cybernetics (SMC)*, 595–602.  
 549 Retrieved from <https://api.semanticscholar.org/CorpusID:5058330>
- 550 Behrens, T. E., & Sporns, O. (2012). Human connectomics. *Current opinion in neurobiology*, 22(1), 144–153.
- 551 Bertolero, M. A., Yeo, B. T. T., & D'Esposito, M. (2015). The modular and integrative functional architecture of the human  
 552 brain. *Proceedings of the National Academy of Sciences*, 112(49), E6798–E6807. Retrieved from  
 553 <https://doi.org/10.1073/pnas.1510619112> doi: 10.1073/pnas.1510619112
- 554 Bihan, D. L., Turner, R., Zeffiro, T. A., Cuenod, C. A., Jezzard, P., & Bonnerot, V. (1993). Activation of human primary  
 555 visual cortex during visual recall: a magnetic resonance imaging study. *Proceedings of the National Academy of Sciences*,  
 556 90(24), 11802–11805. Retrieved from <https://doi.org/10.1073/pnas.90.24.11802> doi:

557 10.1073/pnas.90.24.11802

558 Binder, J. R., Frost, J. A., Hammeke, T. A., Cox, R. W., Rao, S. M., & Prieto, T. (1997). Human brain language areas  
559 identified by functional magnetic resonance imaging. *The Journal of Neuroscience*, 17(1), 353–362. Retrieved from

560 <https://doi.org/10.1523/jneurosci.17-01-00353.1997> doi: 10.1523/jneurosci.17-01-00353.1997

561 Bush, G., & Shin, L. M. (2006). The multi-source interference task: an fMRI task that reliably activates the  
562 cingulo-frontal-parietal cognitive/attention network. *Nature Protocols*, 1(1), 308–313. Retrieved from

563 <https://doi.org/10.1038/nprot.2006.48> doi: 10.1038/nprot.2006.48

564 Chan, M. Y., Alhazmi, F. H., Park, D. C., Savalia, N. K., & Wig, G. S. (2017). Resting-state network topology differentiates  
565 task signals across the adult life span. *The Journal of Neuroscience*, 37(10), 2734–2745. Retrieved from

566 <https://doi.org/10.1523/jneurosci.2406-16.2017> doi: 10.1523/jneurosci.2406-16.2017

567 Churchland, M. M., Cunningham, J. P., Kaufman, M. T., Foster, J. D., Nuyujukian, P., Ryu, S. I., & Shenoy, K. V. (2012).  
568 Neural population dynamics during reaching. *Nature*, 487(7405), 51–56.

569 Cole, M. W., Bassett, D. S., Power, J. D., Braver, T. S., & Petersen, S. E. (2014). Intrinsic and task-evoked network  
570 architectures of the human brain. *Neuron*, 83(1), 238–251. Retrieved from

571 <https://doi.org/10.1016/j.neuron.2014.05.014> doi: 10.1016/j.neuron.2014.05.014

572 Cole, M. W., Ito, T., Schultz, D., Mill, R., Chen, R., & Cocuzza, C. (2019). Task activations produce spurious but systematic  
573 inflation of task functional connectivity estimates. *NeuroImage*, 189, 1-18. Retrieved from

574 <https://www.sciencedirect.com/science/article/pii/S1053811918322043> doi:

575 <https://doi.org/10.1016/j.neuroimage.2018.12.054>

576 Costafreda, S. G., Fu, C. H., Picchioni, M., Toulopoulou, T., McDonald, C., Kravariti, E., ... McGuire, P. K. (2011). Pattern  
577 of neural responses to verbal fluency shows diagnostic specificity for schizophrenia and bipolar disorder. *BMC Psychiatry*,  
578 11(1). Retrieved from <https://doi.org/10.1186/1471-244x-11-18> doi: 10.1186/1471-244x-11-18

579 Coutanche, M. N., & Thompson-Schill, S. L. (2013). Informational connectivity: identifying synchronized discriminability  
580 of multi-voxel patterns across the brain. *Frontiers in human neuroscience*, 7, 15.

581 Craddock, R. C., James, G., Holtzheimer, P. E., Hu, X. P., & Mayberg, H. S. (2011). A whole brain fMRI atlas generated  
582 via spatially constrained spectral clustering. *Human Brain Mapping*, 33(8), 1914–1928. Retrieved from

583 <https://doi.org/10.1002/hbm.21333> doi: 10.1002/hbm.21333

584 Crossley, N. A., Mechelli, A., Vertes, P. E., Winton-Brown, T. T., Patel, A. X., Ginestet, C. E., ... Bullmore, E. T. (2013).

585 Cognitive relevance of the community structure of the human brain functional coactivation network. *Proceedings of the  
586 National Academy of Sciences*, 110(28), 11583–11588. Retrieved from

587 <https://doi.org/10.1073/pnas.1220826110> doi: 10.1073/pnas.1220826110

588 Di, X., & Biswal, B. B. (2017). Psychophysiological interactions in a visual checkerboard task: Reproducibility, reliability,  
589 and the effects of deconvolution. *Frontiers in Neuroscience*, 11. Retrieved from

590 <https://doi.org/10.3389/fnins.2017.00573> doi: 10.3389/fnins.2017.00573

591 Di, X., Reynolds, R. C., & Biswal, B. B. (2017). Imperfect (de)convolution may introduce spurious psychophysiological  
592 interactions and how to avoid it. *Human Brain Mapping*, 38(4), 1723–1740. Retrieved from

593 <https://doi.org/10.1002/hbm.23413> doi: 10.1002/hbm.23413

594 Di, X., Zhang, Z., & Biswal, B. B. (2020). Understanding psychophysiological interaction and its relations to beta series  
595 correlation. *Brain Imaging and Behavior*, 15(2), 958–973. Retrieved from

596 <https://doi.org/10.1007/s11682-020-00304-8> doi: 10.1007/s11682-020-00304-8

597 Ejaz, N., Hamada, M., & Diedrichsen, J. (2015). Hand use predicts the structure of representations in sensorimotor cortex.  
598 *Nature neuroscience*, 18(7), 1034–1040.

599 Esteban, O., Markiewicz, C. J., Blair, R. W., Moodie, C. A., Isik, A. I., Erramuzpe, A., ... Gorgolewski, K. J. (2018).  
600 fMRIprep: a robust preprocessing pipeline for functional MRI. *Nature Methods*, 16(1), 111–116. Retrieved from  
601 <https://doi.org/10.1038/s41592-018-0235-4> doi: 10.1038/s41592-018-0235-4

602 Faskowitz, J., Esfahlani, F. Z., Jo, Y., Sporns, O., & Betzel, R. F. (2020). Edge-centric functional network representations of  
603 human cerebral cortex reveal overlapping system-level architecture. *Nature Neuroscience*, 23(12), 1644–1654. Retrieved  
604 from <https://doi.org/10.1038/s41593-020-00719-y> doi: 10.1038/s41593-020-00719-y

605 Feinberg, T. E., & Farah, M. J. (2006). A historical perspective on cognitive neuroscience. In *Patient-based approaches to  
606 cognitive neuroscience* (p. 3–20). The MIT Press.

607 Finn, E. S., Shen, X., Scheinost, D., Rosenberg, M. D., Huang, J., Chun, M. M., ... Constable, R. T. (2015). Functional  
608 connectome fingerprinting: identifying individuals using patterns of brain connectivity. *Nature Neuroscience*, 18(11),

- 609 1664–1671. Retrieved from <https://doi.org/10.1038/nn.4135> doi: 10.1038/nn.4135
- 610 Fodor, J. A. (1983). *The modularity of mind: An essay on faculty psychology*. Cambridge, MA: MIT Press.
- 611 Fornito, A., Harrison, B. J., Zalesky, A., & Simons, J. S. (2012). Competitive and cooperative dynamics of large-scale brain  
612 functional networks supporting recollection. *Proceedings of the National Academy of Sciences*, 109(31), 12788–12793.  
613 Retrieved from <https://doi.org/10.1073/pnas.1204185109> doi: 10.1073/pnas.1204185109
- 614 Friston, K., Buechel, C., Fink, G., Morris, J., Rolls, E., & Dolan, R. (1997). Psychophysiological and modulatory  
615 interactions in neuroimaging. *NeuroImage*, 6(3), 218–229. Retrieved from  
616 <https://doi.org/10.1006/nimg.1997.0291> doi: 10.1006/nimg.1997.0291
- 617 Friston, K. J. (2011). Functional and effective connectivity: A review. *Brain Connectivity*, 1(1), 13–36. Retrieved from  
618 <https://doi.org/10.1089/brain.2011.0008> doi: 10.1089/brain.2011.0008
- 619 Friston, K. J., Williams, S., Howard, R., Frackowiak, R. S. J., & Turner, R. (1996). Movement-related effects in fMRI  
620 time-series. *Magnetic Resonance in Medicine*, 35(3), 346–355. Retrieved from  
621 <https://doi.org/10.1002/mrm.1910350312> doi: 10.1002/mrm.1910350312
- 622 Gelder, T. V. (1995). What might cognition be, if not computation? *Journal of Philosophy*, 92(7), 345–381. Retrieved from  
623 <https://doi.org/10.2307/2941061> doi: 10.2307/2941061
- 624 Gianaros, P. J., Kraynak, T. E., Kuan, D. C.-H., Gross, J. J., McRae, K., Hariri, A. R., ... Verstynen, T. D. (2020). Affective  
625 brain patterns as multivariate neural correlates of cardiovascular disease risk. *Social Cognitive and Affective Neuroscience*,  
626 15(10), 1034–1045. Retrieved from <https://doi.org/10.1093/scan/nsaa050> doi: 10.1093/scan/nsaa050
- 627 Gianaros, P. J., Rasero, J., DuPont, C. M., Kraynak, T. E., Gross, J. J., McRae, K., ... Barinas-Mitchell, E. (2022).  
628 Multivariate brain activity while viewing and reappraising affective scenes does not predict the multiyear progression of  
629 preclinical atherosclerosis in otherwise healthy midlife adults. *Affective Science*, 3(2), 406–424. Retrieved from  
630 <https://doi.org/10.1007/s42761-021-00098-y> doi: 10.1007/s42761-021-00098-y
- 631 Goldman, M. S., Golowasch, J., Marder, E., & Abbott, L. F. (2001). Global structure, robustness, and modulation of  
632 neuronal models. *Journal of Neuroscience*, 21(14), 5229–5238. Retrieved from  
633 <https://www.jneurosci.org/content/21/14/5229> doi: 10.1523/JNEUROSCI.21-14-05229.2001
- 634 Golowasch, J., Abbott, L. F., & Marder, E. (1999). Activity-dependent regulation of potassium currents in an identified

635 neuron of the stomatogastric ganglion of the crab *cancer borealis*. *Journal of Neuroscience*, 19(20), RC33–RC33.

636 Retrieved from <https://www.jneurosci.org/content/19/20/RC33> doi:

637 10.1523/JNEUROSCI.19-20-j0004.1999

638 Gratton, C., Laumann, T. O., Gordon, E. M., Adeyemo, B., & Petersen, S. E. (2016). Evidence for two independent factors  
639 that modify brain networks to meet task goals. *Cell Reports*, 17(5), 1276–1288. Retrieved from

640 <https://doi.org/10.1016/j.celrep.2016.10.002> doi: 10.1016/j.celrep.2016.10.002

641 Greene, A. S., Gao, S., Scheinost, D., & Constable, R. T. (2018). Task-induced brain state manipulation improves prediction  
642 of individual traits. *Nature Communications*, 9(1). Retrieved from

643 <https://doi.org/10.1038/s41467-018-04920-3> doi: 10.1038/s41467-018-04920-3

644 Hart, H., Marquand, A. F., Smith, A., Cubillo, A., Simmons, A., Brammer, M., & Rubia, K. (2014). Predictive  
645 neurofunctional markers of attention-deficit/hyperactivity disorder based on pattern classification of temporal processing.  
646 *Journal of the American Academy of Child & Adolescent Psychiatry*, 53(5), 569–578.e1. Retrieved from

647 <https://doi.org/10.1016/j.jaac.2013.12.024> doi: 10.1016/j.jaac.2013.12.024

648 Jiang, R., Zuo, N., Ford, J. M., Qi, S., Zhi, D., Zhuo, C., ... Sui, J. (2020). Task-induced brain connectivity promotes the  
649 detection of individual differences in brain-behavior relationships. *NeuroImage*, 207, 116370. Retrieved from  
650 <https://doi.org/10.1016/j.neuroimage.2019.116370> doi: 10.1016/j.neuroimage.2019.116370

651 Just, M. A., Cherkassky, V. L., Buchweitz, A., Keller, T. A., & Mitchell, T. M. (2014). Identifying autism from neural  
652 representations of social interactions: Neurocognitive markers of autism. *PLoS ONE*, 9(12), e113879. Retrieved from  
653 <https://doi.org/10.1371/journal.pone.0113879> doi: 10.1371/journal.pone.0113879

654 Kelso, J. S. (1995). *Dynamic patterns: The self-organization of brain and behavior*.

655 Koch, S. P., Hägele, C., Haynes, J.-D., Heinz, A., Schlagenhauf, F., & Sterzer, P. (2015). Diagnostic classification of  
656 schizophrenia patients on the basis of regional reward-related fMRI signal patterns. *PLOS ONE*, 10(3), e0119089.

657 Retrieved from <https://doi.org/10.1371/journal.pone.0119089> doi: 10.1371/journal.pone.0119089

658 Krakauer, J. W., Ghazanfar, A. A., Gomez-Marin, A., MacIver, M. A., & Poeppel, D. (2017). Neuroscience needs behavior:  
659 correcting a reductionist bias. *Neuron*, 93(3), 480–490.

- 660 Kriegeskorte, N., Mur, M., Ruff, D. A., Kiani, R., Bodurka, J., Esteky, H., ... Bandettini, P. A. (2008). Matching  
661 categorical object representations in inferior temporal cortex of man and monkey. *Neuron*, 60(6), 1126–1141.
- 662 Krienen, F. M., Yeo, B. T. T., & Buckner, R. L. (2014). Reconfigurable task-dependent functional coupling modes cluster  
663 around a core functional architecture. *Philosophical Transactions of the Royal Society B: Biological Sciences*, 369(1653),  
664 20130526. Retrieved from <https://doi.org/10.1098/rstb.2013.0526> doi: 10.1098/rstb.2013.0526
- 665 Lindquist, M. A., Geuter, S., Wager, T. D., & Caffo, B. S. (2019). Modular preprocessing pipelines can reintroduce artifacts  
666 into fMRI data. *Human Brain Mapping*, 40(8), 2358–2376. Retrieved from  
667 <https://doi.org/10.1002/hbm.24528> doi: 10.1002/hbm.24528
- 668 Liu, T. T., Nalci, A., & Falahpour, M. (2017). The global signal in fMRI: Nuisance or information? *NeuroImage*, 150,  
669 213–229. Retrieved from <https://doi.org/10.1016/j.neuroimage.2017.02.036> doi:  
670 10.1016/j.neuroimage.2017.02.036
- 671 Marek, S., Tervo-Clemmens, B., Calabro, F. J., Montez, D. F., Kay, B. P., Hatoum, A. S., ... others (2022). Reproducible  
672 brain-wide association studies require thousands of individuals. *Nature*, 603(7902), 654–660.
- 673 Markello, R. D., & Misic, B. (2021). Comparing spatial null models for brain maps. *NeuroImage*, 236, 118052. Retrieved  
674 from <https://doi.org/10.1016/j.neuroimage.2021.118052> doi: 10.1016/j.neuroimage.2021.118052
- 675 McLaren, D. G., Ries, M. L., Xu, G., & Johnson, S. C. (2012). A generalized form of context-dependent  
676 psychophysiological interactions (gPPI): A comparison to standard approaches. *NeuroImage*, 61(4), 1277–1286.  
677 Retrieved from <https://doi.org/10.1016/j.neuroimage.2012.03.068> doi:  
678 10.1016/j.neuroimage.2012.03.068
- 679 Mourão-Miranda, J., Haroon, D. R., Hahn, T., Marquand, A. F., Williams, S. C., Shawe-Taylor, J., & Brammer, M. (2011).  
680 Patient classification as an outlier detection problem: An application of the one-class support vector machine.  
681 *NeuroImage*, 58(3), 793–804. Retrieved from <https://doi.org/10.1016/j.neuroimage.2011.06.042>  
682 doi: 10.1016/j.neuroimage.2011.06.042
- 683 Newton, A. T., Morgan, V. L., Rogers, B. P., & Gore, J. C. (2010). Modulation of steady state functional connectivity in the  
684 default mode and working memory networks by cognitive load. *Human Brain Mapping*, 32(10), 1649–1659. Retrieved  
685 from <https://doi.org/10.1002/hbm.21138> doi: 10.1002/hbm.21138

- 686 Oby, E. R., Golub, M. D., Hennig, J. A., Degenhart, A. D., Tyler-Kabara, E. C., Byron, M. Y., ... Batista, A. P. (2019). New  
 687 neural activity patterns emerge with long-term learning. *Proceedings of the National Academy of Sciences*, 116(30),  
 688 15210–15215.
- 689 Porro, C. A., Francescato, M. P., Cettolo, V., Diamond, M. E., Baraldi, P., Zuiani, C., ... di Prampero, P. E. (1996). Primary  
 690 motor and sensory cortex activation during motor performance and motor imagery: A functional magnetic resonance  
 691 imaging study. *The Journal of Neuroscience*, 16(23), 7688–7698. Retrieved from  
 692 <https://doi.org/10.1523/jneurosci.16-23-07688.1996> doi: 10.1523/jneurosci.16-23-07688.1996
- 693 Posner, M., Petersen, S., Fox, P., & Raichle, M. (1988). Localization of cognitive operations in the human brain. *Science*,  
 694 240(4859), 1627–1631. Retrieved from <https://doi.org/10.1126/science.3289116> doi:  
 695 10.1126/science.3289116
- 696 Power, J. D., Barnes, K. A., Snyder, A. Z., Schlaggar, B. L., & Petersen, S. E. (2012). Spurious but systematic correlations  
 697 in functional connectivity MRI networks arise from subject motion. *NeuroImage*, 59(3), 2142–2154. Retrieved from  
 698 <https://doi.org/10.1016/j.neuroimage.2011.10.018> doi: 10.1016/j.neuroimage.2011.10.018
- 699 Prinz, A. A., Bucher, D., & Marder, E. (2004). Similar network activity from disparate circuit parameters. *Nature  
 700 Neuroscience*, 7(12), 1345–1352. Retrieved from <https://doi.org/10.1038/nn1352> doi: 10.1038/nn1352
- 701 Rissman, J., Gazzaley, A., & D'Esposito, M. (2004). Measuring functional connectivity during distinct stages of a cognitive  
 702 task. *NeuroImage*, 23(2), 752–763. Retrieved from  
 703 <https://doi.org/10.1016/j.neuroimage.2004.06.035> doi: 10.1016/j.neuroimage.2004.06.035
- 704 Roffman, R. C., Norris, B. J., & Calabrese, R. L. (2012). Animal-to-animal variability of connection strength in the leech  
 705 heartbeat central pattern generator. *Journal of Neurophysiology*, 107(6), 1681–1693. Retrieved from  
 706 <https://doi.org/10.1152/jn.00903.2011> (PMID: 22190622) doi: 10.1152/jn.00903.2011
- 707 Rosenberg, M. D., Finn, E. S., Scheinost, D., Papademetris, X., Shen, X., Constable, R. T., & Chun, M. M. (2015). A  
 708 neuromarker of sustained attention from whole-brain functional connectivity. *Nature Neuroscience*, 19(1), 165–171.  
 709 Retrieved from <https://doi.org/10.1038/nn.4179> doi: 10.1038/nn.4179
- 710 Russo, A. A., Khajeh, R., Bittner, S. R., Perkins, S. M., Cunningham, J. P., Abbott, L. F., & Churchland, M. M. (2020).  
 711 Neural trajectories in the supplementary motor area and motor cortex exhibit distinct geometries, compatible with

- 712 different classes of computation. *Neuron*, 107(4), 745–758.
- 713 Sadtler, P. T., Quick, K. M., Golub, M. D., Chase, S. M., Ryu, S. I., Tyler-Kabara, E. C., ... Batista, A. P. (2014). Neural  
714 constraints on learning. *Nature*, 512(7515), 423–426.
- 715 Schaefer, A., Kong, R., Gordon, E. M., Laumann, T. O., Zuo, X.-N., Holmes, A. J., ... Yeo, B. T. T. (2017). Local-global  
716 parcellation of the human cerebral cortex from intrinsic functional connectivity MRI. *Cerebral Cortex*, 28(9), 3095–3114.  
717 Retrieved from <https://doi.org/10.1093/cercor/bhx179> doi: 10.1093/cercor/bhx179
- 718 Shen, X., Tokoglu, F., Papademetris, X., & Constable, R. (2013). Groupwise whole-brain parcellation from resting-state  
719 fMRI data for network node identification. *NeuroImage*, 82, 403–415. Retrieved from  
720 <https://doi.org/10.1016/j.neuroimage.2013.05.081> doi: 10.1016/j.neuroimage.2013.05.081
- 721 Sheu, L. K., Jennings, J. R., & Gianaros, P. J. (2012). Test-retest reliability of an fMRI paradigm for studies of  
722 cardiovascular reactivity. *Psychophysiology*, 49(7), 873–884. Retrieved from  
723 <https://doi.org/10.1111/j.1469-8986.2012.01382.x> doi: 10.1111/j.1469-8986.2012.01382.x
- 724 Smith, S. M., Fox, P. T., Miller, K. L., Glahn, D. C., Fox, P. M., Mackay, C. E., ... Beckmann, C. F. (2009).  
725 Correspondence of the brain's functional architecture during activation and rest. *Proceedings of the National Academy of  
726 Sciences*, 106(31), 13040-13045. Retrieved from  
727 <https://www.pnas.org/doi/abs/10.1073/pnas.0905267106> doi: 10.1073/pnas.0905267106
- 728 Spadone, S., Penna, S. D., Sestieri, C., Betti, V., Tosoni, A., Perrucci, M. G., ... Corbetta, M. (2015). Dynamic  
729 reorganization of human resting-state networks during visuospatial attention. *Proceedings of the National Academy of  
730 Sciences*, 112(26), 8112–8117. Retrieved from <https://doi.org/10.1073/pnas.1415439112> doi:  
731 10.1073/pnas.1415439112
- 732 Sporns, O. (2013). Network attributes for segregation and integration in the human brain. *Current Opinion in Neurobiology*,  
733 23(2), 162–171. Retrieved from <https://doi.org/10.1016/j.conb.2012.11.015> doi:  
734 10.1016/j.conb.2012.11.015
- 735 Stroop, J. R. (1935). Studies of interference in serial verbal reactions. *Journal of Experimental Psychology*, 18(6), 643–662.  
736 Retrieved from <https://doi.org/10.1037/h0054651> doi: 10.1037/h0054651
- 737 Tetereva, A., Li, J., Deng, J. D., Stringaris, A., & Pat, N. (2022). Capturing brain-cognition relationship: Integrating

- 738 task-based fMRI across tasks markedly boosts prediction and test-retest reliability. *NeuroImage*, 263, 119588. Retrieved  
739 from <https://doi.org/10.1016/j.neuroimage.2022.119588> doi: 10.1016/j.neuroimage.2022.119588
- 740 Wager, T. D., Atlas, L. Y., Lindquist, M. A., Roy, M., Woo, C.-W., & Kross, E. (2013). An fMRI-based neurologic signature  
741 of physical pain. *New England Journal of Medicine*, 368(15), 1388–1397. Retrieved from  
742 <https://doi.org/nejmoa1204471> doi: 10.1056/nejmoa1204471
- 743 Yeo, B. T. T., Krienen, F. M., Eickhoff, S. B., Yaakub, S. N., Fox, P. T., Buckner, R. L., ... Chee, M. W. (2014). Functional  
744 specialization and flexibility in human association cortex. *Cerebral Cortex*, 25(10), 3654–3672. Retrieved from  
745 <https://doi.org/10.1093/cercor/bhu217> doi: 10.1093/cercor/bhu217
- 746 Yoon, J. H., Nguyen, D. V., McVay, L. M., Deramo, P., Minzenberg, M. J., Ragland, J. D., ... Carter, C. S. (2012).  
747 Automated classification of fMRI during cognitive control identifies more severely disorganized subjects with  
748 schizophrenia. *Schizophrenia Research*, 135(1-3), 28–33. Retrieved from  
749 <https://doi.org/10.1016/j.schres.2012.01.001> doi: 10.1016/j.schres.2012.01.001
- 750 Zamani Esfahlani, F., Jo, Y., Faskowitz, J., Byrge, L., Kennedy, D. P., Sporns, O., & Betzel, R. F. (2020). High-amplitude  
751 cofluctuations in cortical activity drive functional connectivity. *Proceedings of the National Academy of Sciences*,  
752 117(45), 28393–28401. Retrieved from <https://www.pnas.org/content/117/45/28393> doi:  
753 10.1073/pnas.2005531117